Nonmixing layers

Pierre Gaillard
ONERA, Chemin de la Hunière, 91123 Palaiseau France

Vincent Giovangigli
CMAP-CNRS, École Polytechnique, 91128 Palaiseau France
and ONERA, Chemin de la Hunière, 91123 Palaiseau France

Lionel Matuszewski
ONERA, Chemin de la Hunière, 91123 Palaiseau France
(Received 28 June 2016; published 12 December 2016)

We investigate the impact of nonideal diffusion on the structure of supercritical cryogenic binary mixing layers. This situation is typical of liquid fuel injection in high-pressure rocket engines. Nonideal diffusion has a dramatic impact in the neighborhood of chemical thermodynamic stability limits where the components become quasi-immiscible and ultimately form a nonmixing layer. Numerical simulations are performed for mixing layers of H_2 and N_2 at a pressure of 100 atm and temperature around 120–150 K near chemical thermodynamic stability limits.

DOI: 10.1103/PhysRevFluids.1.084001

I. INTRODUCTION

The injection of reactants in cryogenic combustion engines is often performed at supercritical pressure [1,2]. Experimental studies have been devoted to such high-pressure injection phenomena in reactive [1,2] and nonreactive [3] situations and numerical simulations of laminar [4–9] and turbulent supercritical flames [10–12] have been conducted. At such cryogenic conditions, however, nonideal effects may strongly influence fuel mixing properties at injection or inside locally extinguished fuel pockets. With such motivations, we investigate in this work the impact of nonideal diffusion on supercritical mixing layers of H_2 and N_2.

Dense fluid models are generally based on thermodynamics of irreversible processes [13–18], statistical mechanics [19–21], statistical thermodynamics [22], or the kinetic theory of dense gases [23–25]. The fluid model used in this work combines a real gas thermodynamics based on the cubic Soave-Redlich-Kwong equation of state [26–33] with nonideal transport fluxes [7]. The Soave-Redlich-Kwong (SRK) equation of state is widely used for the modeling of transcritical flows and yields a good representation of dense to dilute fluids [5,7].

The corresponding thermodynamics is obtained by further using the compatibility with perfect gases at low densities [28]. An important consequence of such nonideal thermodynamics is the presence of thermodynamic instabilities that may be of thermal, mechanical, or chemical type [7].

The entropy of a stable isolated homogeneous system should indeed be a concave function of its thermodynamic variables. Whenever it is not the case, the system loses its homogeneity and splits between two or more phases in order to reach equilibrium. The stability condition associated with the entropy Hessian matrix may be decomposed into thermal, mechanical, and chemical stability conditions [28]. The thermal stability condition is generally guaranteed by the SRK equation of state [28] and the mechanical condition is associated with liquid-vapor instability for single species fluids. The chemical stability condition states that the Hessian matrix of the Gibbs function at constant pressure and temperature should be positive semidefinite with null space given by the homogeneity condition [9,28]. Analysis of thermodynamic stability conducted for supercritical

flames has further shown that as pressure is reduced, chemical instabilities generally appear before mechanical instabilities [9] and this has motivated the choice of such chemical instabilities in order to investigate mixing layers.

Equilibrium mixtures of H_2 and N_2 at high pressure and low temperature have been investigated experimentally by Verschoyle [34] and Eubanks [35]. In such situations, a mixture of H_2 and N_2 may split between a hydrogen-rich gaseouslike phase and a hydrogen-poor liquidlike phase [34,35]. Detailed comparisons have been conducted between experimental results and numerical simulations of equilibrium states using the SRK equation of state [7,28]. These simulations have confirmed that such instabilities are of chemical type and very good agreement has been obtained with experimental results [7]; this has motivated us to focus on mixtures of H_2 and N_2.

Molecular transport fluxes for dense fluid are naturally expressed in terms of gradients of chemical potentials [7,18,22,24]. Such nonideal fluxes ensure the positivity of entropy production associated with transport [7]. Nonideality in diffusion driving forces have already been considered by Okong'o and Bellan [4], Oefelein [10], Bellan [11], and Giovangigli *et al.* [7]. Transport nonidealities are notably strong in cold zones of premixed flames and prevent unrealistic diffusion from dense fresh reactants into flame fronts [7]. Nonideal diffusion also has a strong influence on the structure of counterflow cold jets near chemical thermodynamic stability limits between two fluids [8]. There is a need, however, for investigating the impact of nonideal diffusion on the structure of mixing layers typical of fuel rocket injection.

The exact multicomponent matrix solution of Stefan-Maxwell-like equations is expressed in terms of the mixture binary diffusion coefficient $\mathcal{D}_{12}$ and the thermodynamic matrix associated with nonideality is also expressed in terms of a single thermodynamic coefficient γ. This coefficient γ is unity for ideal gases and vanishes at chemical thermodynamic stability limit. Exact matrix diffusion processes for nonideal binary mixtures are shown to coincide with the Fick diagonal-type diffusion model provided it is written with a mass-based thermodynamic coefficient γ and in term of mass fraction gradients.

Mixing layers between cryogenic H_2 and N_2 at supercritical pressure are studied numerically. Nonidealities in diffusion driving forces have a dramatic influence near thermodynamical instability. The quasinonmiscibility of H_2 and N_2 for high pressure and low temperature results in stiff mole fraction gradients inside the mixing layer and the appearance of a quasi-interface in contrast with the mild gradients of the erroneous ideal transport solution. Using ideal diffusion models further leads to mixing layer structures in which some unstable, and thus unphysical, thermodynamical states appear in the computational domain.

II. NONIDEAL MIXING LAYER

The equations governing steady self-similar nonideal mixing layers are presented.

A. Governing equations

We consider a binary mixing layer developing in the positive x direction starting from $x = 0$, where x and y denote the longitudinal and transverse coordinates. Using the simplified coordinates $\xi = x$ and $\zeta = y/x^{1/2}$, the equations governing steady self-similar binary mixing layers are in the form

$$\partial_\zeta(\rho w) + \tfrac{1}{2}\rho u = 0, \tag{1}$$

$$\rho w \partial_\zeta u - \partial_\zeta(\eta \partial_\zeta u) = 0, \tag{2}$$

$$\rho w \partial_\zeta \mathsf{y}_1 - \partial_\zeta(\rho\gamma\mathcal{D}_{12}\partial_\zeta \mathsf{y}_1) = 0, \tag{3}$$

$$\rho w \partial_\zeta h - \partial_\zeta[\lambda\partial_\zeta T + \rho(h_1 - h_2)\gamma\mathcal{D}_{12}\partial_\zeta \mathsf{y}_1] = 0, \tag{4}$$

where ρ denotes the mass density, u is the longitudinal velocity, $w = \sqrt{\xi}\, v - \frac{1}{2}\zeta u$ is the auxiliary velocity, v is the transverse velocity, η is the shear viscosity, y_1 is the mass fraction of the first species, γ is the mass-based thermodynamic coefficient, $\mathcal{D}_{12}$ is the binary diffusion coefficient between the species pair, h is the enthalpy of the mixture, λ is the thermal conductivity, and h_1 and h_2 are the species enthalpies. The transverse mass flux $-\rho\gamma\mathcal{D}_{12}\partial_\zeta \mathsf{y}_1$ arises from the expression of the species diffusion flux

$$\mathcal{J}_1 = -\rho\gamma\mathcal{D}_{12}\nabla\mathsf{y}_1, \tag{5}$$

derived from nonideal Stefan-Maxwell relations in Appendix A, and the thermodynamic coefficient is discussed in Sec. II C. The thermal conductivity λ and the shear viscosity η are evaluated as described by Chung *et al.* [36] and Ely and Hanley [37] and the binary diffusion coefficient $\mathcal{D}_{12}$ is obtained from the kinetic theory of dense mixtures of hard spheres developed by Van Beijeren and Ernst [24] and Kurochkin *et al.* [25]. This binary diffusion coefficient reads $\mathcal{D}_{12} = \mathcal{D}_{12}^{\mathrm{PG}}/\Upsilon_{12}$, where $\mathcal{D}_{12}^{\mathrm{PG}}$ is the dilute gas binary diffusion coefficient [38–43] and

$$\Upsilon_{12} = 1 + \sum_{k\in\{1,2\}} \frac{\pi \mathfrak{n}_k}{12}\left[8\left(\sigma_{1k}^3 + \sigma_{2k}^3\right) - 6\left(\sigma_{1k}^2 + \sigma_{2k}^2\right)\sigma_{12} - 3\left(\sigma_{1k}^2 - \sigma_{2k}^2\right)^2\sigma_{12}^{-1} + \sigma_{12}^3\right],$$

where σ_{ij} denotes the collision diameter for the species pair (i,j) and $\mathfrak{n}_k$ the number density of the kth species.

The computational domain is typically taken in the form $[\mathcal{L}_\zeta^-, \mathcal{L}_\zeta^+]$, with the boundary conditions in the form

$$u(\mathcal{L}_\zeta^-) = u_-, \quad T(\mathcal{L}_\zeta^-) = T_-, \quad \mathsf{y}_1(\mathcal{L}_\zeta^-) = 1,$$

$$u(\mathcal{L}_\zeta^+) = u_+, \quad T(\mathcal{L}_\zeta^+) = T_+, \quad \mathsf{y}_1(\mathcal{L}_\zeta^+) = 0,$$

and the Ting boundary condition for the transverse velocity reads [44,45]

$$\rho_- u_- v_- + \rho_+ u_+ v_+ = 0.$$

The low-Mach-number approximation has been used inEqs. (1)–(4) and the pressure decomposed in the form $p = \overline{p} + \widetilde{p}$, where $\overline{p}$ denotes the ambient pressure constant in space and $\widetilde{p}$ the fluid mechanical perturbation with $\widetilde{p}/\overline{p}$ of the order of the square of the Mach number [38]. Since the limiting longitudinal velocities $u(\pm\infty)$ are independent of x, we have $\partial_\xi \widetilde{p} = 0$ and combining with the transverse momentum equation $\partial_\zeta \widetilde{p} = 0$, it is found that $\nabla\widetilde{p} = 0$, so

$\widetilde{p} = 0$ with a suitable boundary condition and the pressure is constant $p = \overline{p}$.

B. Nonideal thermodynamics

The Soave-Redlich-Kwong equation of state [26,27] may be written

$$p = \sum_{i\in\mathfrak{S}} \frac{\mathsf{y}_i}{m_i}\frac{RT}{v-b} - \frac{a}{v(v+b)}, \tag{6}$$

where p denotes the pressure, $\mathfrak{S}$ the species indexing set, R the perfect gas constant, y_i the mass fraction of the ith species, $v = 1/\rho$ the volume per unit mass, a the massic attractive parameter, and b the massic repulsive parameter. The mass fraction of the ith species may be written $\mathsf{y}_i = \rho_i/\rho$ and the vector of species mass fractions is denoted by $\mathsf{y} = (\mathsf{y}_1, \ldots, \mathsf{y}_n)^t$. The parameters of the SRK equation of state $a(\mathsf{y}_1, \ldots, \mathsf{y}_n, T)$ and $b(\mathsf{y}_1, \ldots, \mathsf{y}_n)$ are evaluated from the van der Waals mixing rules $a = \sum_{i,j\in\mathfrak{S}} \mathsf{y}_i\mathsf{y}_j\alpha_i\alpha_j$ and $b = \sum_{i\in\mathfrak{S}} \mathsf{y}_i b_i$. The pure-component parameters $\alpha_i(T)$ and b_i are obtained from critical point data [7]. The validity of this equation of state (6) and of the mixing rules have been carefully studied by comparison with NIST data by Congiunti *et al.* [29] and with the results of Monte Carlo simulations by Colonna and Silva [30] and Cañas-Marín *et al.* [31,32]. This

cubic equation of state yields a good representation of dense to dilute fluids and still allows a fast inversion by using Cardan's formula.

With the pressure law (6) given, there exists a unique associated Gibbsian thermodynamics compatible at low densities with that of perfect gases [28,33]. For the Soave-Redlich-Kwong equation of state it is possible to evaluate analytically the corresponding mixture thermodynamic functions. In particular, the enthalpy h and the Gibbs function g per unit mass are found in the form

$$h = \sum_{i\in\mathfrak{S}} \mathsf{y}_i \left(h_i^{\rm st} + \int_{T^{\rm st}}^{T} c_{{\rm p}i}^{\rm PG}(\theta) d\theta \right) + \frac{T\partial_T a - a}{b} \ln\left(1+\frac{b}{v}\right) + \sum_{i\in\mathfrak{S}} \frac{\mathsf{y}_i}{m_i} \frac{RTb}{v-b} - \frac{a}{v+b}, \tag{7}$$

$$g = \sum_{i\in\mathfrak{S}} \mathsf{y}_i \left(h_i^{\rm st} + \int_{T^{\rm st}}^{T} c_{{\rm p}i}^{\rm PG}(\theta) d\theta - T s_i^{\rm st} - T\int_{T^{\rm st}}^{T} \frac{c_{{\rm p}i}^{\rm PG}(\theta)}{\theta} d\theta \right) + \sum_{i\in\mathfrak{S}} \mathsf{y}_i \frac{RT}{m_i} \ln\left(\frac{\mathsf{y}_i RT}{m_i (v-b) p^{\rm st}} \right)$$
$$+ \sum_{i\in\mathfrak{S}} \frac{\mathsf{y}_i}{m_i} \frac{RTb}{v-b} - \frac{a}{b} \ln\left(1+\frac{b}{v}\right) - \frac{a}{v+b}, \tag{8}$$

where $h_i^{\rm st}$ is the standard formation enthalpy of the ith species per unit mass at the standard temperature $T^{\rm st}$, $s_i^{\rm st}$ is the formation entropy of the ith species per unit mass at the standard temperature $T^{\rm st}$ and standard pressure $p^{\rm st}$, and $c_{{\rm p}i}^{\rm PG}$ is the perfect-gas specific heat at constant pressure of the ith species.

C. Chemical thermodynamic stability

The entropy of a stable isolated homogeneous system should be a concave function of its thermodynamic variables $w = (v, \mathsf{y}_1, \ldots, \mathsf{y}_n, e)^t$. Whenever it is not the case, the system loses its homogeneity and splits between two or more phases in order to reach equilibrium. The Hessian matrix $\partial^2_{ww} s$ must therefore be negative semi-definite with null space $N(\partial^2_{ww} s) = \mathbb{R}\, w$ associated with homogeneity [38]. One may establish that thermodynamic stability holds if and only if the following properties hold:

$$(\partial_T e)_{v,\mathsf{y}} > 0, \quad (\partial_v p)_{T,\mathsf{y}} < 0, \quad \big(\partial^2_{\mathsf{yy}} g\big)_{T,p} \geqslant 0, \quad N\big[\big(\partial^2_{\mathsf{yy}} g\big)_{T,p}\big] = \mathbb{R}\mathsf{y}. \tag{9}$$

The first condition $(\partial_T e)_{v,\mathsf{y}} > 0$ is the thermal stability condition that generally holds with the SRK equation of state [28]. The second condition $(\partial_v p)_{T,\mathsf{y}} < 0$ is the mechanical stability condition associated with liquid-vapor phase changes in single-species fluids. The third condition is the chemical stability condition and states that the Hessian matrix of the Gibbs function per unit mass $\mathcal{G} = (\partial^2_{\mathsf{yy}} g)_{T,p}$ should be positive semidefinite with null space given by $N(\mathcal{G}) = \mathbb{R}\mathsf{y}$ from homogeneity. The two last conditions, mechanical and chemical, are equivalent to the combined property that the matrix $(\partial^2_{\mathsf{yy}} g)_{T,v}$ is positive definite [28]. Analysis of thermodynamic stability in the supercritical flame has shown that, as pressure is reduced, chemical instabilities always appear before mechanical instabilities [9]. Moreover, in unstable zones, there generally exists a unique positive eigenvalue of the Hessian matrix of entropy [9]. Mechanical stability limits also introduce numerous singularities in the coefficients of the governing equations [9].

Since the Gibbs function per unit mass g is 1-homogeneous in terms of y, when T and p are constant, the derivatives g_i, $i \in \mathfrak{S}$, with respect to mass fractions are 0-homogeneous, so $\mathcal{G}_{11}\mathsf{y}_1 + \mathcal{G}_{12}\mathsf{y}_2 = 0$ and $\mathcal{G}_{21}\mathsf{y}_1 + \mathcal{G}_{22}\mathsf{y}_2 = 0$ from the Euler relation. Introducing the mass-based coefficient

$$\gamma = -\mathcal{G}_{12}\frac{m_1 m_2}{mRT} = -\big(\partial_{\mathsf{y}_1}\mu_2\big)_{T,p}\frac{m_1}{m} = -\big(\partial_{\mathsf{y}_2}\mu_1\big)_{T,p}\frac{m_2}{m}, \tag{10}$$

we may then rewrite $\mathcal{G}$ in the form

$$\mathcal{G} = \frac{mRT}{m_1 m_2}\gamma \begin{pmatrix} \frac{\mathsf{y}_2}{\mathsf{y}_1} & -1 \\ -1 & \frac{\mathsf{y}_1}{\mathsf{y}_2} \end{pmatrix}. \tag{11}$$

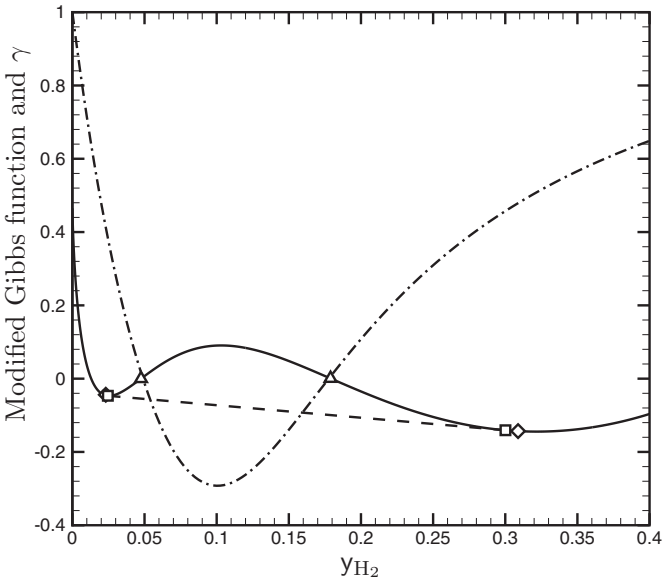

FIG. 1. Modified Gibbs function and coefficient γ as a function of the hydrogen mole fraction in a H_2-N_2 mixture at pressure $p = 95.2$ atm and temperature $T = 83.15$ K:—, modified Gibbs function; - · -, coefficient γ; - - -, bitangent; △, chemical stability limits; □, numerical simulation of equilibrium points; and ◇, experimental measurements of equilibrium points.

It is then easily established that $\mathcal{G} \geqslant 0$ is equivalent to $\gamma \geqslant 0$ and $N(\mathcal{G}) = \mathbb{R}\mathsf{y}$ is equivalent to $\gamma \neq 0$ using that $\langle \mathcal{G}z,z\rangle = \gamma mRT/m_1m_2\mathsf{y}_1\mathsf{y}_2$, where $z = (1,-1)^t$. Therefore, thermodynamic stability holds if and only if $\gamma > 0$ and a direct calculation yields that $\gamma = 1$ for perfect gases. When γ is negative, there is a spinodal decomposition between the two equilibrium states characterized by the bitangent condition. In this situation $\gamma < 0$, higher-order derivative terms from the second gradient theory of diffuse interfaces are required in order to stabilize mathematically the governing equations [9] and in order to simulate numerically unmixing processes. Moreover, from (5) it is clear that the diffusion processes vanishes at the chemical stability limit $\gamma = 0$.

Verschoyle [34] and Eubanks [35] have established experimentally that binary mixtures of H_2 and N_2 are not thermodynamically stable at sufficiently high pressure and low temperature. In these situations, a mixture of H_2 and N_2 splits between a hydrogen-rich gaseouslike phase and a hydrogen-poor liquidlike phase [7,28,34,35]. Among the experimental measurements presented by Eubanks [35], the situation where $p = 95.2$ atm and $T = 83.15$ K is considered. Figure 1 presents the corresponding modified Gibbs function $\widehat{g} = 10^{-8}g + 470.00\mathsf{y}_{H_2} + 66.05$ and the factor γ as a function of the hydrogen mass fraction y_{H_2}. The modified Gibbs function $\widehat{g}$ has been selected in order to emphasize the loss of convexity and in order to show the points where stability is lost on the horizontal axis.

Figure 1 illustrates that the mixture is no longer stable at these conditions, as shown by the loss of convexity between the point indicated by the triangle symbol. These points correspond to the inflection points of the Gibbs function g and of the modified Gibbs function $\widehat{g}$. These points also coincide with the points where the factor γ vanishes, in agreement with the theory. We have also indicated with square symbols the equilibrium solutions calculated with the SRK equation of state [7]. These equilibrium points are such that there exists a bitangent line to the $\mathsf{y}_{H_2} \rightarrow \widehat{g}(\mathsf{y}_{H_2})$ curve. The experimental measurements of equilibrium points by Eubanks [35] are also presented with diamonds and the agreement between theory and experiment is very good, keeping in mind that there are no adjustable parameters.

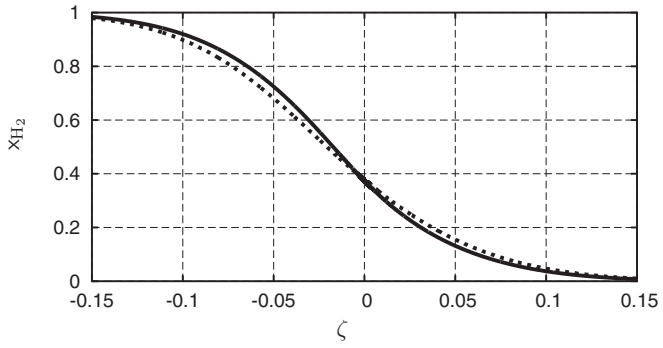

FIG. 2. Hydrogen mole fraction in a mixing layer at $\overline{p} = 100$ atm and $T_{\pm} = 160$ K:—, nonideal diffusion; - - -, ideal diffusion.

III. NUMERICAL SIMULATIONS

Binary mixing layers of H_2 and N_2 near thermodynamic stability limits are simulated numerically.

A. Numerical considerations

The set of equations is discretized by using finite differences and solved on self-adaptive grids with Newton's method [46,47]. Pseudounsteady iterations may also be used used to provide an inaccurate initial guess in the convergence domain of the steady Newton iteration. The grid is iteratively refined by adding discretization points wherever the solution gradients are too roughly represented. The evaluation of fluid properties such as chemical production rate, thermodynamic properties, and transport coefficient is obtained with high-pressure adapted versions of highly optimized thermochemistry and transport routines [48–51].

B. Structure of the mixing layer

A mixing layer between H_2 and N_2 is investigated in a configuration far from chemical thermodynamic stability limit. The species indexing set $\mathfrak{S} = \{H_2, N_2\}$ is also used for convenience. Hydrogen is injected on the left side $\mathsf{y}_{1-} = \mathsf{y}_{H_2-} = 1$, at temperature $T_- = 160$ K, and longitudinal velocity $u_- = 1$ cm/s, and the pressure is uniform at $\overline{p} = 100$ atm. Nitrogen is on the right side $\mathsf{y}_{1+} = \mathsf{y}_{H_2+} = 0$, at temperature $T_+ = 160$ K, and longitudinal velocity $u_+ = 1$ cm/s. Taking into account the governing equation for u and the boundary conditions $u_- = u_+ = 1$ cm/s, the

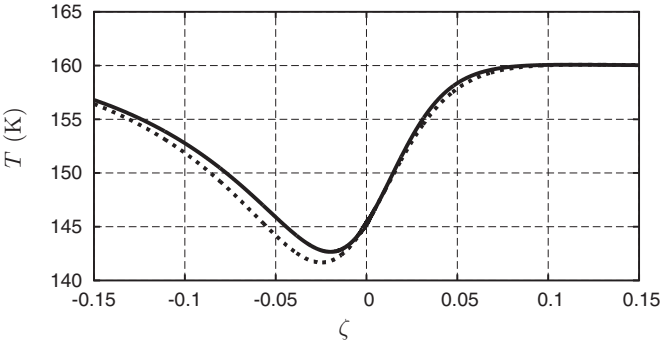

FIG. 3. Temperature in a mixing layer at $\overline{p} = 100$ atm and $T_{\pm} = 160$ K:—, nonideal diffusion; - - -, ideal diffusion.

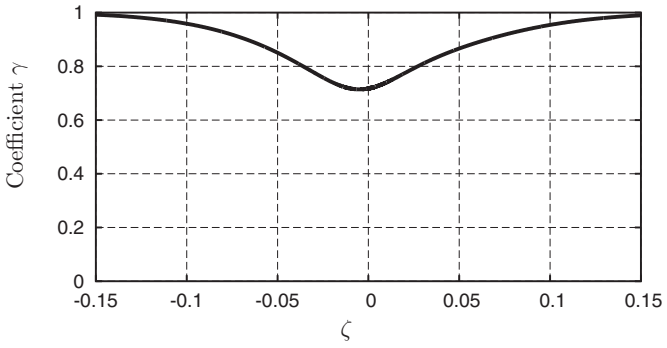

FIG. 4. Coefficient γ in a mixing layer at $\overline{p} = 100$ atm and $T_{\pm} = 160$ K.

longitudinal velocity is found to be constant $u = 1$ cm/s. The domain in the transformed coordinate ζ is typically given by $[-0.28, 0.28]$ and Fig. 2 presents the hydrogen mole fraction $\mathsf{x}_1(\zeta) = \mathsf{x}_{\mathrm{H}_2}(\zeta)$ as a function of the self-similar transverse coordinate ζ.

The ideal diffusion mole fraction profile is the dashed curve and the nonideal one is the solid curve. We can see that, at such temperatures, the impact of nonidealities, although measurable, remains unessential. Figure 3 presents the temperature profiles as a function of ζ and we can see the influence of nonidealities in the temperature variations arising through the dependence of partial enthalpies h_1 and h_2 on the species mass fractions and on density. The corresponding coefficient γ is presented in Fig. 4 and this coefficient significantly deviates from unity but still remains away from zero with a minimum value around $\gamma \approx 0.714$.

C. Impact of nonideal transport

A mixing layer between H_2 and N_2 near the chemical thermodynamic stability limit is investigated in this section. The geometry is similar to that of the previous section with the hydrogen on the left $\mathsf{y}_{1-} = \mathsf{y}_{\mathrm{H}_2-} = 1$, injected at temperature $T_- = 122$ K, with $u_- = 1$ cm/s, and the pressure is uniform at $p = \overline{p} = 100$ atm. The boundary conditions on the nitrogen side on the right are $\mathsf{y}_{1+} = \mathsf{y}_{\mathrm{H}_2+} = 0$, with $T_+ = 122$ K and $u_+ = 1$ cm/s. The main difference from the situation of Sec. III B is the colder temperature $T_{\pm} = 122$ K at both ends that will result in the mixture near the chemical thermodynamic stability limit. This can be seen in Fig. 5, where the coefficient γ comes very close to zero near the chemical thermodynamic stability limit. This coefficient now has a minimum value around $\gamma \approx 3.5 \times 10^{-3}$, much lower than the previous minimum value of γ obtained with temperature $T_{\pm} = 160$ K.

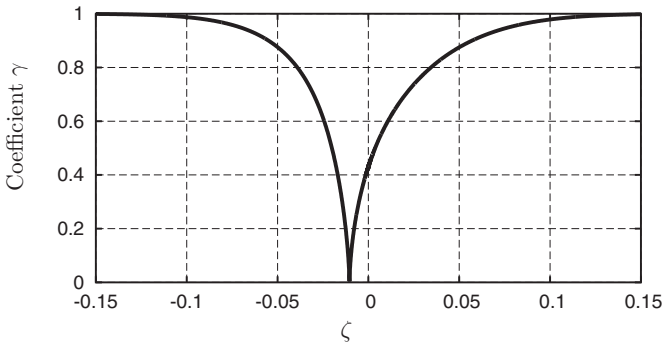

FIG. 5. Coefficient γ in a mixing layer at $\overline{p} = 100$ atm and $T_{\pm} = 122$ K.

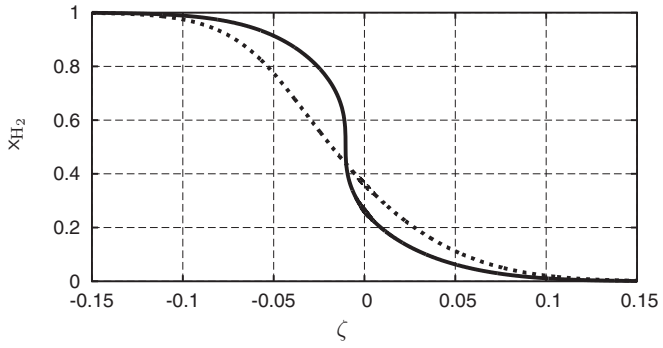

FIG. 6. Hydrogen mole fraction in a mixing layer at $\overline{p} = 100$ atm and $T_{\pm} = 122$ K:—, nonideal diffusion; - - -, ideal diffusion.

Figure 6 presents the hydrogen mole fraction $\mathsf{x}_{\mathrm{H}_2}$ as a function of ζ for both the ideal and nonideal models. The ideal diffusion mole fraction is the dashed curve and the nonideal one is the solid curve. We can see that, at such temperatures, the impact of nonidealities is dramatic. The nonideal diffusion mole fraction profile is much stiffer than the ideal diffusion one near the chemical thermodynamic stability limit where the thermodynamic factor γ vanishes. The sharp gradient of the mole fraction is due to the local quasi-immiscibility of the two fluids. The limiting structure is then that of a contact discontinuity or, equivalently, that of a nonmixing layer. An important consequence is the considerable decrease of mixing processes in such systems and the ideal model is unable to properly describe the relevant physics of diffusion. Figure 7 represents the temperature profiles as a function of ζ with again an important influence of nonideal diffusion.

The trajectories in the phase space $(\mathsf{x}_{\mathrm{H}_2}, T)$ corresponding to the three limiting boundary temperatures $T_{\pm} = 160$, 140, and 122 K are finally presented in Fig. 8. In this phase diagram, the isocontours $\gamma = 0.00$, 0.25, 0.50, and 0.75 of the parameter γ are also presented, as well as the forbidden zone $\gamma < 0$, where the binary mixture is thermodynamically unstable, which is represented by the gray region. It has already been observed that only nonideal diffusion fluxes properly represent the physics of diffusion near thermodynamic stability. However, it is also observed in Fig. 8 that, with ideal diffusion fluxes, the forbidden unstable zone is crossed without even noticing it when $T_{\pm} = 122$ K. In contrast, with the nonideal model, all trajectories remain in the physically admissible stable zone.

When the temperature is further decreased, thermodynamic stability is lost and two separate phases appear. It is then necessary to use a a second gradient model of Cahn-Hilliard or van de Waals–Korteweg type in order to avoid a discontinuous representation of the fluid. In the

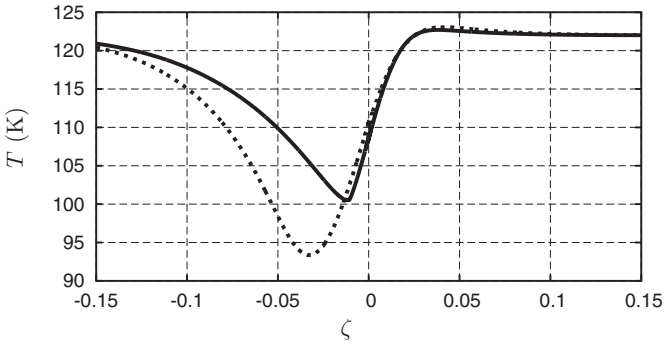

FIG. 7. Temperature in a mixing layer at $\overline{p} = 100$ atm and $T_{\pm} = 122$ K:—, nonideal diffusion; - - -, ideal diffusion.

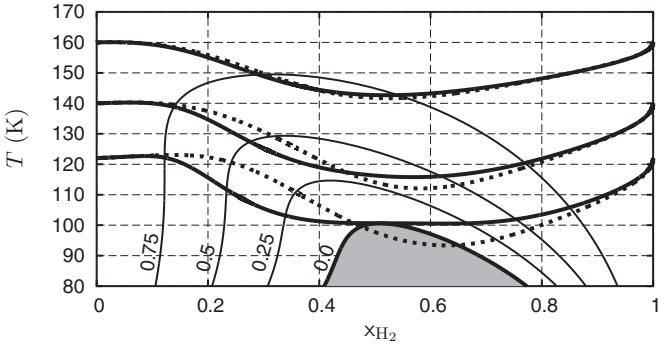

FIG. 8. Phase diagram with mixing layer trajectories at $\overline{p} = 100$ atm and $T_{\pm} = 160$, 140, and 122 K, and γ isocontours;—, nonideal diffusion; - - -, ideal diffusion;—, γ isocontours. The thermodynamic unstable zone $\gamma < 0$ is in gray.

unstable thermodynamic zone, indeed, both the hyperbolicity and parabolicity of the system of partial differential equations are lost. The square of the sound velocity may be negative, as well as entropy production due to diffusion, and the single fluid model without extra stabilizing effects cannot be used anymore.

The inconsistent model where a nonideal thermodynamic is used with ideal diffusion fluxes may also lead to numerical problems. Generally speaking, since hyperbolicity is lost in the unstable thermodynamic region, it may lead to a number of difficulties when solving the Riemann problem [52]. These difficulties are not encountered in this work because of the simpler structure of the mixing layers. For lower pressures, mechanical stability is also lost and such instabilities may also lead to numerical difficulties.

IV. CONCLUSION

Nonideal binary diffusion fluxes have been analyzed and the influence of thermodynamics were shown to arise through a single coefficient mass-based γ multiplying the binary diffusion coefficient $\mathcal{D}_{12}$. The influence of thermodynamics on the structure of mixing layers of H_2 and N_2 near chemical thermodynamic stability limits has been shown to be essential. Moreover, ideal diffusion models do not even realize the presence of unphysical thermodynamically unstable points.

APPENDIX A: TRANSPORT FLUXES

Neglecting thermal diffusion effects, the species diffusion fluxes $\mathcal{J}_i, i \in \mathfrak{S}$, and the heat flux $\mathcal{J}_e$ are in the form

$$\mathcal{J}_i = -\sum_{j\in\mathfrak{S}} \rho \mathsf{y}_i D_{ij} \boldsymbol{d}_j, \quad i \in \mathfrak{S} \tag{A1}$$

$$\mathcal{J}_e = -\lambda \nabla T + \sum_{i\in\mathfrak{S}} h_i \mathcal{J}_i, \tag{A2}$$

where $\boldsymbol{d}_j$ denotes the diffusion driving force of the jth species; $D_{ij}, i,i \in \mathfrak{S}$, are the multicomponent diffusion coefficients; and λ is the thermal conductivity gase [7,39–42]. Soret and Dufour effects generally have a moderate influence [7] and the mixing layers considered in this work only involve mild temperature gradients. The species diffusion driving forces read $\boldsymbol{d}_j = \mathsf{x}_j(\nabla\mu_j)_T$, where x_j is the mole fraction of the jth species and $(\nabla\mu_j)_T$ is the gradient of the chemical potential μ_j with the temperature held constant. In the low-Mach-number limit the diffusion driving forces may further be simplified as $\boldsymbol{d}_j = \mathsf{x}_j(\nabla\mu_j)_{T,p} = \sum_{l\in\mathfrak{S}} \frac{\mathsf{y}_j m}{RT} \mathcal{G}_{jl} \nabla \mathsf{y}_l$, $j \in \mathfrak{S}$, where $\mathcal{G}_{jl} = (\partial^2_{\mathsf{y}_j \mathsf{y}_l} g)_{T,p}$.

The kinetic theories of mixtures of dilute gases [38–42] and of dense gases [25] show that the multicomponent diffusion matrix D may be obtained from the Stefan-Maxwell matrix Δ by solving $\Delta D = \mathsf{I} - \mathsf{y}\otimes\mathsf{u}$ with the mass constraints $D\mathsf{y} = 0$. For a binary mixture, the Stefan-Maxwell matrix reduces to

$$\Delta = \frac{\mathsf{x}_1\mathsf{x}_2}{\mathcal{D}_{12}}\begin{pmatrix} 1 & -1 \\ -1 & 1 \end{pmatrix} \tag{A3}$$

and using $\mathsf{y}_1 D_{11} + \mathsf{y}_2 D_{12} = 0$, $\mathsf{y}_1 D_{21} + \mathsf{y}_2 D_{22} = 0$, $D_{12} = D_{21}$, and $\Delta D = \mathsf{I} - \mathsf{y}\otimes\mathsf{u}$, it is obtained that $D_{12} = -\mathcal{D}_{12} m_1 m_2/m^2$, so

$$D = \mathcal{D}_{12}\frac{m_1 m_2}{m^2}\begin{pmatrix} \frac{\mathsf{y}_2}{\mathsf{y}_1} & -1 \\ -1 & \frac{\mathsf{y}_1}{\mathsf{y}_2} \end{pmatrix}; \tag{A4}$$

it is easily checked that D is positive semidefinite with null space $\mathbb{R}\mathsf{y}$. From (A1), (A4), and (11) and using $\mathsf{y}_1 + \mathsf{y}_2 = 1$ and $\nabla\mathsf{y}_1 = -\nabla\mathsf{y}_2$, it is found that

$$\mathcal{J}_1 = -\rho\mathcal{D}_{12}\gamma\mathsf{y}_1\left\{\frac{\mathsf{y}_2}{\mathsf{y}_1}\mathsf{y}_1\left(\frac{\mathsf{y}_2}{\mathsf{y}_1}+1\right) - \mathsf{y}_2\left(-1-\frac{\mathsf{y}_1}{\mathsf{y}_2}\right)\right\}\nabla\mathsf{y}_1$$

and finally, after some algebra, that (5) holds.

APPENDIX B: SIMPLIFIED LAYER EQUATIONS

Two-dimensional boundary layer equations are first derived in the low-Mach-number regime by assuming that the transverse derivatives are more significant than longitudinal derivatives. The resulting dissimilar mixing layer governing equations are found in the form

$$\partial_x(\rho u) + \partial_y(\rho v) = 0, \tag{B1}$$

$$\rho u\partial_x u + \rho v\partial_y u = -\partial_x\widetilde{p} + \partial_y(\eta\partial_y u), \tag{B2}$$

$$\partial_y\widetilde{p} = 0, \tag{B3}$$

$$\rho u\partial_x\mathsf{y}_1 + \rho v\partial_y\mathsf{y}_1 = \partial_y(\rho\mathcal{D}_{12}\gamma\partial_y\mathsf{y}_1), \tag{B4}$$

$$\rho u\partial_x h + \rho v\partial_y h = \partial_y[\lambda\partial_y T + \rho\mathcal{D}_{12}\gamma(h_1 - h_2)\partial_y\mathsf{y}_1]. \tag{B5}$$

In order to obtain the equations governing self-similar mixing layers, we introduce the simplified variables

$$\tau = t, \quad \xi = x, \quad \zeta = y/x^{1/2}, \tag{B6}$$

which are much simpler than traditional boundary-layer-type variables. Then, for any smooth function $\phi(t,x,y)$, setting $\widehat{\phi}(\tau,\xi,\zeta) = \phi(t,x,y)$, the following differential relations hold:

$$\partial_t\phi = \partial_\tau\widehat{\phi}, \quad \partial_x\phi = \partial_\xi\widehat{\phi} - \frac{\zeta}{2\xi}\partial_\zeta\widehat{\phi}, \quad \partial_y\phi = \xi^{-1/2}\partial_\zeta\widehat{\phi}, \tag{B7}$$

$$\partial_\tau\widehat{\phi} = \partial_t\phi, \quad \partial_\xi\widehat{\phi} = \partial_x\phi + \frac{y}{2x}\partial_y\phi, \quad \partial_\zeta\widehat{\phi} = x^{1/2}\partial_y\phi, \tag{B8}$$

and the governing equations (1)–(4) are obtained after some algebra by further using $\partial_\xi = 0$ due to self-similarity and $\partial_\tau = 0$ since the flow is steady.

[1] M. Habiballah, M. Orain, F. Grisch, L. Vingert, and P. Gicquel, Experimental studies of high pressure cryogenic flames on the MASCOTTE facility, Combust. Sci. Technol. **178**, 101 (2006).
[2] S. Candel, M. Juniper, G. Singla, P. Scouflaire, and C. Rolon, Structure and dynamics of cryogenic flames at supercritical pressure, Combust. Sci. Technol. **178**, 161 (2006).
[3] B. Chehroudi, D. Talley, and E. Coy, Visual characteristics and initial growth rates of round cryogenic jets at subcritical and supercritical pressures, Phys. Fluids **14**, 850 (2002).
[4] N. A. Okong'o and J. Bellan, Direct numerical simulation of a transitional supercritical binary mixing layer: Heptane and nitrogen, J. Fluid Mech. **464**, 1 (2002).
[5] G. Ribert, N. Zong, V. Yang, L. Pons, N. Darabiha, and S. Candel, Counterflow diffusion flames of general fluids: Oxygen/hydrogen mixtures, Combust. Flame **154**, 319 (2008).
[6] L. Pons, N. Darabiha, S. Candel, G. Ribert, and V. Yang, Mass transfer and combustion in transcritical non-premixed counterflows, Combust. Theory Model. **13**, 57 (2009).
[7] V. Giovangigli, L. Matuszewski, and F. Dupoirieux, Detailed modeling of transcritical planar H_2-O_2-N_2 flames, Combust. Theory Model. **15**, 141 (2011).
[8] V. Giovangigli and L. Matuszewski, Numerical simulation of transcritical strained laminar flames, Combust. Flame **159**, 2829 (2012).
[9] P. Gaillard, V. Giovangigli, and L. Matuszewski, A transcritical diffuse interface H_2/LOX flame model, Combust. Theory Model. **20**, 486 (2016).
[10] J. C. Oefelein, Thermophysical characteristics of shear-coaxial LOX-H_2 flames at supercritical pressure, Proc. Combust. Inst. **30**, 2929 (2005).
[11] J. Bellan, Theory, modeling and analysis of turbulent supercritical mixing, Combust. Sci. Technol. **178**, 253 (2006).
[12] T. Schmitt, Y. Méry, M. Boileau, and S. Candel, Large-eddy simulation of oxygen/methane flames under transcritical conditions, Proc. Combust. Inst. **33**, 1383 (2011).
[13] L. Onsager, Reciprocal relations in irreversible processes, Phys. Rev. **37**, 405 (1931).
[14] C. Eckart, The thermodynamic of irreversible processes, II. Fluid mixtures, Phys. Rev. **58**, 269 (1940).
[15] J. Meixner, Zur thermodynamik der thermodiffusion, Ann. Phys. (Leipzig) **431**, 333 (1941).
[16] J. Meixner, Zur thermodynamik der irreversiblen prozesse in gasen mit chemisch reagierenden, dissoziierenden und anregbaren komponenten, Ann. Phys. (Leipzig) **435**, 244 (1943).
[17] I. Prigogine, *Etude Thermodynamique des Phénomènes Irréversibles* (Dunod, Paris, 1947).
[18] S. R. de Groot and P. Mazur, *Non-Equilibrium Thermodynamics* (Dover, New York, 1984).
[19] J. H. Irving and J. G. Kirkwood, The statistical mechanics of transport processes. IV. The equations of hydrodynamics, J. Chem. Phys. **18**, 817 (1950).
[20] R. J. Bearman and J. G. Kirkwood, The statistical mechanics of transport processes. XI. Equations of transport in multicomponent systems, J. Chem. Phys. **28**, 136 (1958).
[21] H. Mori, Statistical-mechanical theory of transport in fluids, Phys. Rev. **112**, 1829 (1958).
[22] J. Keizer, *Statistical Thermodynamics of Nonequilibrium Processes* (Springer, New York, 1987).
[23] L. Bajaras, L. S. Garcia-Colin, and E. Piña, On the Enskog-Thorne theory for a binary mixture of dissimilar rigid spheres, J. Stat. Phys. **7**, 161 (1973).
[24] H. Van Beijeren and M. H. Ernst, The modified Enskog equations for mixtures, Physica **70**, 225 (1973).
[25] V. I. Kurochkin, S. F. Makarenko, and G. A. Tirskii, Transport coefficients and the Onsager relations in the kinetic theory of dense gas mixtures, J. Appl. Mech. Tech. Phys. **25**, 218 (1984).
[26] O. Redlich and J. N. S. Kwong, On the thermodynamics of solutions. V. An equation of state. Fugacities of gaseous solutions, Chem. Rev. **44**, 233 (1949).
[27] G. S. Soave, Equilibrium constants from a modified Redlich-Kwong equation of state, Chem. Eng. Sci. **27**, 1197 (1972).
[28] V. Giovangigli and L. Matuszewski, Supercritical fluid thermodynamics from equations of state, Physica D **241**, 649 (2012).
[29] A. Congiunti, C. Bruno, and E. Giacomazzi, in *Proceedings of the 41th Aerospace Sciences Meeting and Exhibit* (AIAA, Reston, 2003), paper AIAA-2003-478.

[30] P. Colonna and P. Silva, Dense gas thermodynamic properties of single and multicomponent fluids for fluid dynamics simulations, J. Fluid Eng. **125**, 414 (2003).
[31] W. A. Cañas-Marín, U. E. Guerrero-Aconcha, and J. D. Ortiz-Arango, Comparison of different cubic equations of state and combination rules for predicting residual chemical potential of binary and ternary Lennard-Jones mixtures, Fluid Phase Equil. **234**, 42 (2005).
[32] W. A. Cañas-Marín, J. D. Ortiz-Arango, U. E. Guerrero-Aconcha, and C. P. Soto-Tavera, Thermodynamic derivative properties and densities for hyperbaric gas condensates: SRK equation of state predictions versus Monte Carlo data, Fluid Phase Equil. **253**, 147 (2007).
[33] R. C. Reid, J. M. Prausnitz, and B. E. Poling, *The Properties of Gases and Liquids* (McGraw-Hill, New York, 1987).
[34] T. T. H. Verschoyle, The ternary system monoxide-nitrogen-hydrogen and the component binary systems between temperatures of −185 degrees and −215 degrees C., and between pressures of 0 and 225 atm, Philos. Trans. R. Soc. London Ser. A **230**, 189 (1932).
[35] L. S. Eubanks, *Vapor-Liquid Equilibria in the System Hydrogen-Nitrogen-Carbon Monoxide* (The Rice Institute, Houston, 1957).
[36] T. H. Chung, M. Ajlan, L. L. Lee, and K. E. Starling, Generalized multiparameter correlation for nonpolar and polar fluid transport properties, Ind. Eng. Chem. Res. **27**, 671 (1988).
[37] J. F. Ely and H. J. Hanley, Prediction of transport properties. 2. Thermal conductivity of pure fluids and mixtures, Ind. Eng. Chem. Fund. **22**, 90 (1983).
[38] V. Giovangigli, *Multicomponent Flow Modeling* (Birkhaüser, Boston, 1999).
[39] L. Waldmann, *Thermodynamik der Gase*, edited by S. Flügge, Handbuch der Physik Vol. 3 (Springer, Berlin, 1958), p. 295.
[40] S. Chapman and T. G. Cowling, *The Mathematical Theory of Non-Uniform Gases* (Cambridge University Press, Cambridge, 1970).
[41] J. H. Ferziger and H. G. Kaper, *Mathematical Theory of Transport Processes in Gases* (North-Holland, Amsterdam, 1972).
[42] A. Ern and V. Giovangigli, *Multicomponent Transport Algorithms*, Lecture Notes in Physics Monographs, Vol. 24 (Springer, Heidelberg, 1994).
[43] V. Giovangigli and L. Matuszewski, Mathematical modeling of supercritical multicomponent reactive fluids, Math. Mod. Meth. Appl. Sci. **23**, 2193 (2013).
[44] L. Ting, On the mixing of two parallel streams, J. Math. Phys. **38**, 153 (1959).
[45] C. A. Kennedy and T. B. Gatski, Self-similar supersonic variable density shear layers in binary systems, Phys. Fluids **6**, 662 (1994).
[46] M. D. Smooke, Solution of burner stabilized premixed laminar flames by boundary value methods, J. Comput. Phys. **48**, 72 (1982).
[47] M. D. Smooke, The computation of laminar flames, Proc. Combust. Inst. **34**, 65 (2013).
[48] R. Bendakhlia, V. Giovangigli, and D. Rosner, Soret effects in laminar counterflow spray diffusion flames, Combust. Theory Model. **6**, 1 (2002).
[49] V. Giovangigli and N. Darabiha, in *Mathematical Modeling in Combustion and Related Topics*, edited by C.-M. Brauner and C. Schmidt-Lainé, NATO Advanced Studies Institute, Series E: Applied Sciences (Nijhoff, Dordrecht, 1988), Vol. 140, pp. 491–503.
[50] A. Ern and V. Giovangigli, EGlib server and User's manual, http://www.cmap.polytechnique.fr/www.eglib
[51] L. Matuszewski, Ph.D. thesis, University Paris 6, 2011.
[52] R. Menikoff and B. J. Plohr, The Riemann problem for fluid flow of real materials, Rev. Mod. Phys. **61**, 75 (1989).